Open Journal of Fluid Dynamics, **2013, 3, 100-107**
http://dx.doi.org/10.4236/ojfd.2013.32A016 Published Online July 2013 (http://www.scirp.org/journal/ojfd)

A Study of Thermal Response and Flow Field Coupling Simulation around Hayabusa Capsule Loaded with Light-Weight Ablator

Hisashi Kihara, Naoya Hirata, Ken-ichi Abe
Department of Aeronautics and Astronautics, Kyushu University, Fukuoka, Japan
Email: kihara@aero.kyushu-u.ac.jp

Received July 17, 2013; revised August 15, 2013; accepted August 29, 2013

ABSTRACT

The numerical simulation of flow field around Hayabusa capsule loaded with light-weight ablator thermal response coupled with pyrolysis gas flow inside the ablator was carried out. In addition, the radiation from high temperature gas around the capsule was coupled with flow field. Hayabusa capsule reentered the atmosphere about 12 km/sec in velocity and Mach number about 30. During such an atmospheric entry, space vehicle is exposed to very savior aerodynamic heating due to convection and radiation. In this study, Hayabusa capsule was treated as a typical model of the atmospheric entry spacecraft. The light-weight ablator had porous structure, and permeability was an important parameter to analyze flow inside ablator. In this study, permeability was a variable parameter dependent on density of ablator. It is found that the effect of permeability of light-weight ablator was important with this analysis.

Keywords: Light-Weight Ablator; Coupling Calculation; Pyrolysis Gas Flow; Hayabusa Capsule

1. Introduction

About the space mission in near future, it is expected that the sample return mission like Stardust and Hayabusa increases. In those missions, the space vehicle reenters to atmosphere at very high speed. In an atmospheric entry condition, a strong shock wave and a high enthalpy flow field are generated around the flight vehicle. For example, Hayabusa reentry capsule, which returned to Earth in 2010, had the velocity of about 12 km/sec and experienced the heating rate of about 20 MW/m^2 [1]. To protect an entry vehicle from such a severe aerodynamic heating, thermal protection system (TPS) is one of the key components in its design. Especially, an ablator has been widely used as a TPS material for a vehicle under such a high-heating condition. In addition, in such high enthalpy flow, the estimation of heat flux from flow to the vehicle is very complex and difficult. Although a carbon ablator is known as an often-used one, its heaviness had been a critical problem in considering the severe weight limitation of a space vehicle. However, a light-weight ablator named phenolic impregnated carbon ablator (PICA) was developed at NASA Ames Research Center in 1990's and used for the Stardust sample return capsule fore body heat shield. Its density is lower than 300 kg/m^3 [2], while most of the conventional carbon ablators have the density of over 1000 kg/m^3.

In Japan, a light-weight ablator (300 - 400 kg/m^3) for middle range heat flux is being developed in JAXA [3]. These light-weight ablators will become more and more important for expanding the capability of future missions and thus sophisticated numerical models are needed to predict their thermal response more correctly.

An ablator under severe heating environment involves several complex physics. When the ablator is heated, the inside resin pyrolyzes and the pyrolysis gas is generated. Then, the pyrolysis gas flow through the ablator, which is porous media, ejects from its surface to the outer flow field. This flow contributes to reduction of the heat flux to the ablator surface. Furthermore, the pyrolysis of the resin that is endothermic reaction contributes to cooling the ablator itself. From these characteristics, the ablator can be used as an effective passive thermal protection. However, the aforesaid complex phenomena are involved in its analysis and thus there still remain uncertainties in predicting the thermal response of the ablator. Several efforts have focused on identifying thermal response of an ablator. Charring Materials Ablation (CMA) code and Fully Implicit Ablation and Thermal response (FIAT)

program [4] simulated the internal heat conduction and the thermal decomposition in one dimension. More sophisticated simulation code named Two-dimensional Implicit Thermal response and Ablation (TITAN) [5] enabled two-dimensional simulation.

On the other hand, Ahn H. *et al*. developed a computational code named Super Charring Materials Ablation (SCMA) [6]. In SCMA code, the motion of the pyrolysis gas inside an ablator was simulated in one dimension by solving the mass and momentum equations for the gas phase. Suzuki T. *et al*. extended SCMA code for two dimensional simulation and named the code (SCMA2) [7]. Moreover, they coupled SCMA2 code with a CFD code using the Park's two-temperature model and chemical reactions with 21 species for a thermochemical nonequilibrium flow [8].

In our research group, numerical and experimental studies have been conducted for determining the thermal response of a light-weight ablator exposed to a flow field generated by an arc-heated wind tunnel, which is often used for a heating test of an ablator [9-11]. Therefore, in the present study, the thermal response simulation code is extended so that it can treat the pyrolysis gas flow as unsteady phenomena in two-dimensional axisymmetric coordinate. Besides, the CFD code is also extended so as to include more chemical species, leading to more detailed evaluation of the ablation-gas injection consisting of the pyrolysis gas and the carbonaceous gas generated by the surface reactions. Furthermore, the code is developed for application to wider range of the flow conditions not only for a nitrogen flow but also for an air flow.

2. Computational Models

To simulate the process of heat shield using ablator, we have to treat many complex situations like the blowing flow of pyrolysis gas from ablator, chemical reaction on the surface recession of ablator, radiation heat conduction from strong shock heated gas, and interaction between blowout gas and free stream, etc. To understand such complex phenomena, the coupling simulation of outer flow-field and inside of ablator was employed.

2.1. Flow-Fields

Flow-field is assumed continuous and axisymmetric flow. Navier-Stokes equation extends to thermo-chemical non-equilibrium flow is adopted as governing equation. The present simulation treats 11 species (N_2, O_2, NO, N_2^+, O_2^+, NO^+, N, O, N^+, O^+, e^-) for free stream and 9 species (H_2, C_2, C_3, CN, CO, H, C, H^+, C^+) are related to ablation gas. These 20 Species and 153 chemical reactions are considered [12].

The four temperature model is employed to handle in detail thermal non-equilibrium. These are translation, rotation, vibration and electron respectively. The electro excited temperature treats as equilibrium to electron temperature. The energy transfers between each of the internal energy modes are considered as follows: translation-rotation [13], translation-vibration [14], translation-electron [15,16], rotation-vibration [13], rotation-electron [17] and vibration-electron [18]. The energy losses for vibration and rotation due to the heavy particle-impact dissociation [16] and the electron energy loss due to the electron-impact dissociation/ionization reactions are considered. In addition, radiated heat transfer is not ignored, so the radiation field of high temperature gas is calculated coupled with flow field around capsule. For the calculation of radiation field, the present paper employed 3-band model [19] extended to chemical nonequilibrium flow field, which is very low cost method [20].

The char layer at the ablator surface is lost due to the surface reactions and then the ablator surface recedes. The recession rate r is determined using the carbon mass loss rate:

$$r = \frac{1}{\rho_{char}}\left(\frac{M_C}{M_{CN}} J_{CN}^{nit} + \frac{M_C}{M_{CO}} J_{CO}^{oxi} + \frac{M_C}{M_C} J_C^{sub} + \frac{M_C}{M_{C2}} J_{C2}^{sub} + \frac{M_C}{M_{C3}} J_{C3}^{sub} \right) \quad (1)$$

The shape change should be accounted in the simulation because the magnitude and distribution of the heat flux are very sensitive to the surface shape [21]. Thus, in order to consider the shape change due to the surface recession, the computational domains for both the ablator and the flow field are reconstructed according to the surface recession. In this calculation, the grid system was rebuilt at the each 1 μm recession quantity.

2.2. Thermal Response of Ablator

In this simulation, the ablator is made of carbon foam material impregnated with phenolic resin. It is easy predicted that the flow of pyrolysis gas inside the light-weight ablator was different because it had much vacant spaces. The permeability of virgin layer of conventional ablator has quite little compare with the permeability of light-weight ablator's one. Therefore, it is considered the phenomena inside the ablator include the conversion from the solid to the gas phases (pyrolysis), the heat conduction in the solid and the gas phases and the gas phase flow with convective heat transfer. The governing equations inside ablator are shown as follows.

Solid mass conservation:

$$\frac{\partial \rho_s}{\partial t} = -R \quad (2)$$

Solid energy conservation:

$$\frac{\partial E_s}{\partial t}=\frac{\partial}{\partial x_j}\left(\lambda_s\frac{\partial T_s}{\partial x_j}\right)-Q_{sg}-R\cdot e_s+(1-a)R\Delta h^{pyr} \quad (3)$$

Gas mass conservation

$$\frac{\partial(\varepsilon\rho_g)}{\partial t}+\frac{\partial}{\partial x_j}(\varepsilon\rho_g u_i)=-R \quad (4)$$

Gas momentum conservation

$$\frac{\partial(\varepsilon\rho_g u_j)}{\partial t}+\frac{\partial}{\partial x_j}(\varepsilon\rho_g u_i u_j+\varepsilon\delta_{ij}p)=\frac{\partial(\varepsilon\tau_{ji})}{\partial x_j}-\varepsilon f_i \quad (5)$$

Gas energy conservation

$$\begin{aligned}&\frac{\partial(\varepsilon E_g)}{\partial t}+\frac{\partial}{\partial x_j}\left[\varepsilon(E_g+p)u_j\right]\\&=\frac{\partial}{\partial x_j}\left[\varepsilon u_i\tau_{ji}+\varepsilon\lambda_g\frac{\partial T_g}{\partial x_j}\right]+Q_{sg}+R\cdot e_g+aR\Delta h^{pyr}\end{aligned} \quad (6)$$

where subscripts *s* and *g* represent the solid and the gas phases, respectively.

In Equation (2), R represents the pyrolysis rate. It shows as follow [22]:

$$R=-\left(\frac{\partial(\rho_s)}{\partial t}\right)=A\exp\left(-\frac{B}{T_s}\right)\rho_{\text{virgin}}\left(\frac{\rho_s-\rho_{char}}{\rho_{\text{virgin}}}\right) \quad (7)$$

In Equations (3) and (6), a represent the effectiveness of reaction heat for gas phase and $(1-a)$ is for solid phases respectively. The third term in Equation (3) and fourth term in Equation (6) represents the energy exchange between the solid and the gas phases. The fourth term in Equation (3) and fifth term in Equation (6) are the energy loss and energy gain due to the pyrolysis, respectively. The last term in Equations (3) and (6) are the source terms due to the reaction heat of the pyrolysis. The pyrolysis gas made from C, H, O and calculated by chemical equilibrium code [23].

The solid phase consists of char and resin and then the solid density is given by the sum of those densities:

$$\rho=\rho_{resin}+\rho_{char} \quad (8)$$

Note that the char density ρ_{char} is constant, while the resin density ρ_{resin} decreases by the pyrolysis. Similarly, the internal energy of the solid phase is divided into the parts of char and resin:

$$E_s=\rho_{resin}e_{resin}+\rho_{char}e_{char} \quad (9)$$

$$e_{resin}=\int C_{p,resin}(T)\,\mathrm{d}T+\Delta h^0_{resin} \quad (10)$$

$$e_{char}=\int C_{p,char}(T)\,\mathrm{d}T+\Delta h^0_{char} \quad (11)$$

The specific heat is given in the form proposed by Potts [24]. This form is based on the characteristics that the specific heat of graphite.

$$C_{p,s}=C_\infty\frac{T_s}{\sqrt{T_s^2+(C_\infty/c_1)}} \quad (12)$$

where C_∞ and c_1 are determined by curve fitting based on JANAF's data sheet of graphite [25].

The pressure of the gas phase is given by the equation of state:

$$p=\rho_g RT_g \quad (13)$$

The internal energy of the gas phase is given by

$$E_g=\rho_g e_g=\rho_g\left(C_v T_g+\Delta h_g^0+\frac{1}{2}q^2\right) \quad (14)$$

where $q^2=u_i u_i$.

The thermal conductivity is determined by a curve-fitting method with a manufacturing data sheet on carbon fiber material. Porosity is given by

$$\varepsilon=\varepsilon_{\min}-\frac{\rho_{\text{virgin}}-\rho_s}{\rho^*_{resin}} \quad (15)$$

where $\varepsilon_{\min}$ represents the porosity in case that the resin before pyrolyzes.

The friction force per unit volume $\boldsymbol{f}$ is given by

$$\boldsymbol{f}=\mu\boldsymbol{K}^{-1}\boldsymbol{u} \quad (16)$$

where $\boldsymbol{K}$ is the permeability tensor.

$$\boldsymbol{K}=\begin{bmatrix}\cos\theta & -\sin\theta\\ \sin\theta & \cos\theta\end{bmatrix}\begin{bmatrix}K_1 & 0\\ 0 & K_2\end{bmatrix}\begin{bmatrix}\cos\theta & \sin\theta\\ -\sin\theta & \cos\theta\end{bmatrix} \quad (17)$$

θ is the direction along the capsule surface for lightweight ablator or the laminated direction for conventional ablator. K_1 is the permeability of θ direction, and K_2 is the normal direction of θ. K_1 and K_2 are measured by experiment in our laboratory.

2.3. Coupling and Conditions

The analysis of Flow field and thermal response of the ablator coupling is done through the boundary condition of these two fields. The boundary conditions change time after time. The reentry trajectory determined by JAXA [26] is treated in present study. The calculation condition shows in **Table 1**. Time 0sec was altitude at 200 km. The calculation was done during 40 sec to 100 sec for ablator. As the boundary condition of inflow, pseudo steady condition is used. Inflow boundary condition changed every 5 sec. The calculation conditions are shown in **Table 1**.

Numerical domain is shown in **Figure 1**. The computation mesh are 110 × 60 for flow field and 60 × 60 for ablator.

3. Result and Discussions

Figure 2 shows temperatures distribution along center

Table 1. Free stream conditions at calculated point.

Flight time S	Altitude Km	Velocity km/s	Density kg/m^3	Temperature K
55	77.75	11.695	2.408×10^{-5}	213.7
60	68.59	11.546	9.065×10^{-5}	226.8
65	59.94	11.061	2.897×10^{-4}	242.3
70	52.16	9.868	7.785×10^{-4}	256.4
75	45.74	7.807	1.785×10^{-3}	258.1
80	40.99	5.422	3.516×10^{-3}	247.7

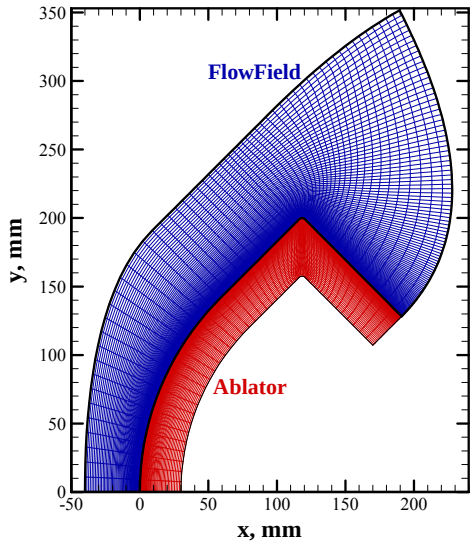

Figure 1. Numerical grid system.

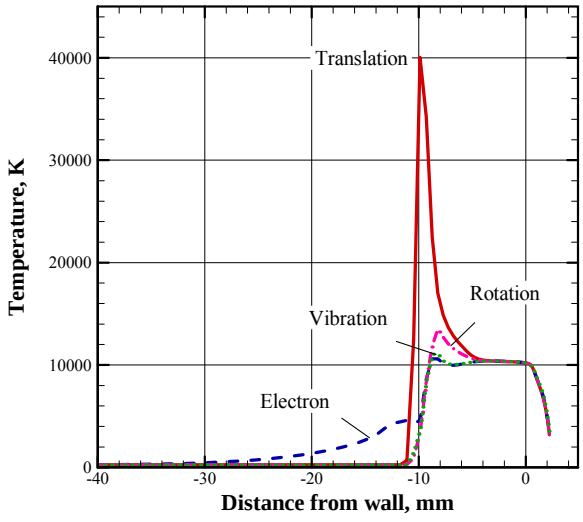

Figure 2. On axis temperatures distribution at 52.16 km.

axis in front of vehicle at 52.12 km in altitude and 70 sec after reentry as a typical condition. We discuss about condition 52.12 km which the typical data of present simulation. The zero point of x-axis shows the initial position of capsule surface. A precursor is remarkably seen because gas becomes a very high temperature with the shock wave. The numerical domain of flow field is selected that the effect of precursor could not ignore. The translational temperature becomes about 40,000 K. It can be seen that it is the strong thermal nonequilibrium upstream than 5 mm of initial surface. The temperature of the plateau part behind shock wave exceeds 10,000 K and the four temperatures are almost equilibrium.

Figure 3 shows temperatures distribution along center shows the difference in the temperature profiles along the centerline without ablator or ablator. The zero point of x-axis shows the surface of capsule. To be easy to look, only translational temperature and vibrational temperature are shown here. There seems to be no difference between two conditions. However, the peak translational temperature and the temperature gradient of approach to the surface are different and this difference indicates ablating cooling.

Figure 4 shows temperature profiles for each time along the center line using heavy ablator. The calculation started t = 40 sec cause of the heat flux is enough small to able to ignore. At t = 40 sec to 60 sec, it assumed that the heat flux and pressure interpolated by quadratic function. On the other hand, it assumed that the heat flux became 0 at t = 100 and calculation was stopped. The peak temperature of the surface is about 3100 K at 70 sec. This value has good agreement with measured value [26] when Hayabusa reentered.

Figures 5 and **6** show pressure distribution and mass flux vectors of pyrolysis gas for heavy ablator and lightweight ablator at 52.16 km, respectively. The permeability of conventional heavy ablator at virgin layer is quite large so that the pyrolysis gas could not penetrate to the direction of rear wall. So the pyrolysis gas must flow out

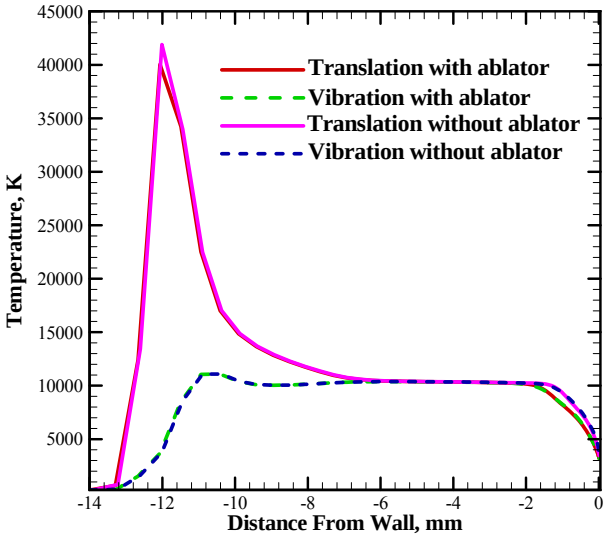

Figure 3. Difference of temperatures distribution between with and without ablated flow at 52.16 km.

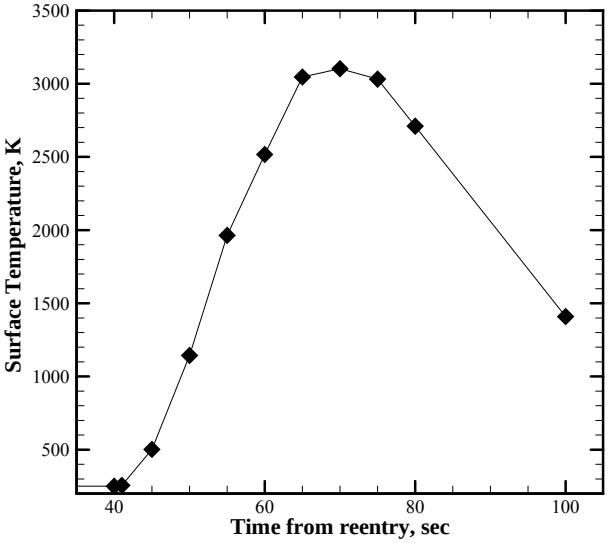

Figure 4. Surface temperature history at stagnation with heavy ablator.

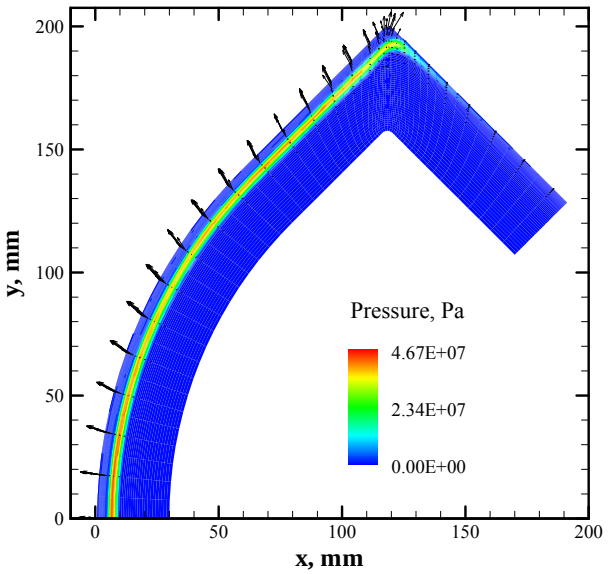

Figure 5. Pressure distribution and mass flux vectors of pyrolysis gas at 52.16 km with heavy ablator.

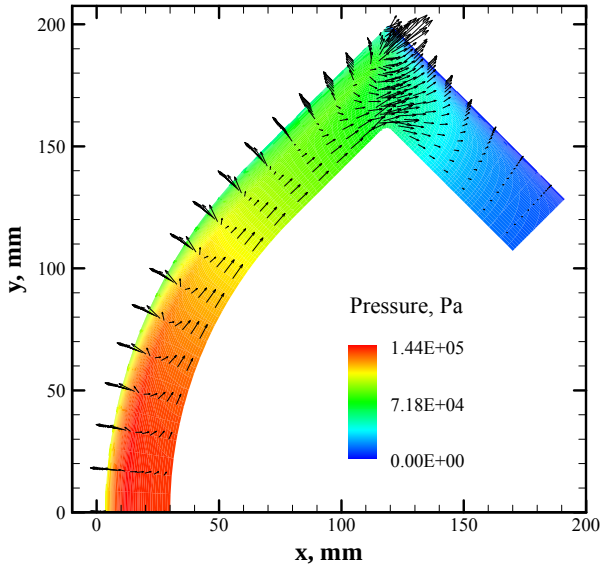

Figure 6. Pressure distribution and mass flux vectors of pyrolysis gas at 52.16 km with light-weight ablator.

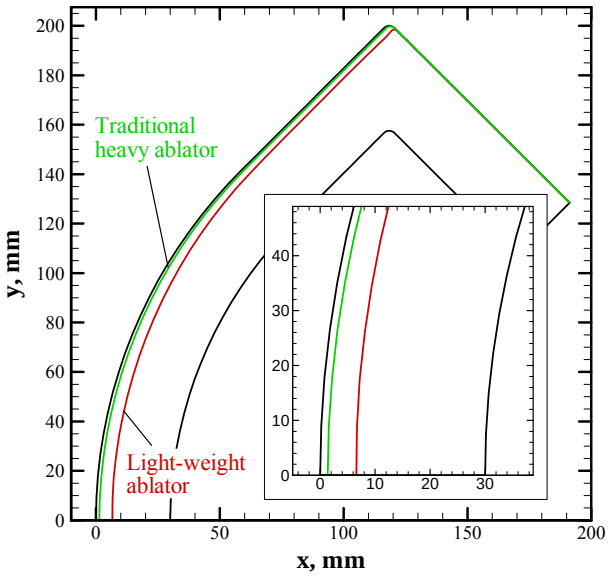

Figure 7. Shape change of ablator at 100 sec.

to front side only. On the other hand, the pyrolysis gas inside light-weight ablator flows not only front but also rear and radial direction. The pyrolysis gas in light-weight ablator is more transmissible than heavy weight ablator. Therefore, the pressure distribution of pyrolysis-gas in light-weight type became broad. In addition, cause of the anisotropy of permeability (distribution of porosity) the flow to the radial direction is occurred strongly. Particularly, the flow of the shoulder part in the ablator is influenced strong by the expansion wave from the corner.

The shapes of ablator surface at 100 sec are shown in **Figure 7**. The black line is the initial line, the green line and the red line show heavy ablator and light-weight ablator respectively.

The zooming up around stagnation region is imposed. The quantity of the recession at stagnation point is large for high heat flux. However, extreme change of shape does not occur and it keeps similarity shape mainly. The recessions of surface at stagnation point at 100 sec of heavy ablator and light-weight ablator are 1.4 mm and 6.6 mm respectively. In addition, the surface temperature at 100 sec is between 1300 K and 1450 K. The surface recession does not occur dramatically in such temperature region. On the other hand, there is little the surface recession at side wall. The temperature of side wall is not more than about 1000 K. The total surface recession at

stagnation point has predicted with 2 mm from 1 mm by Suzuki *et al*. [26]. The present study has good agreement to heavy ablator. **Figure 8** shows the history of convective heat flux at stagnation point. The Solid lines show conventional heat flux and the black line shows non ablated wall condition for compared. The radiative equilibrium condition is used at the surface condition. Green and red lines are heavy and light-weight respectively. The dashed line shows net heat flux with surface chemical reaction that includes surface reactions (nitrization, oxization, sublimation). The effusion of pyrolysis gas works effectively to decrease heat flux. The dashed lines are higher than 30% of solid lines. We can see that the surface reaction play important role. In comparison with it, the difference between heavy ablator and light-weight ablator is not so much. On the other hand, radiative heat flux (**Figure 9**) does not decrease using by ablating material. It rather increase slightly cause of radiation from ablating species. It can find a very slight difference between heavy ablator and light-weight ablator in radiative heat flux.

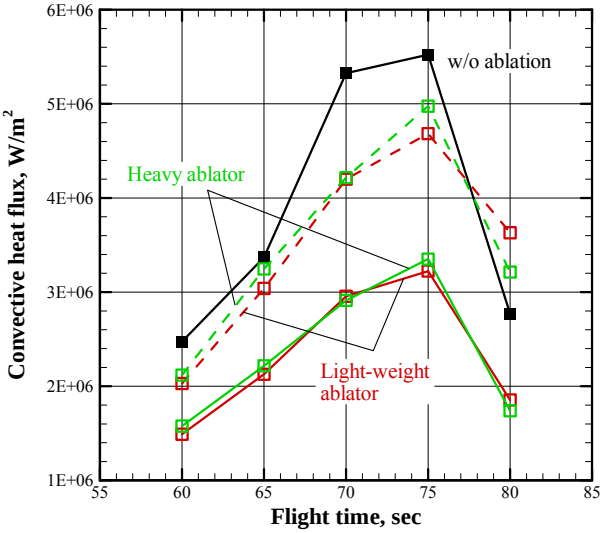

Figure 8. Time profiles of convective heat flux at stagnation point.

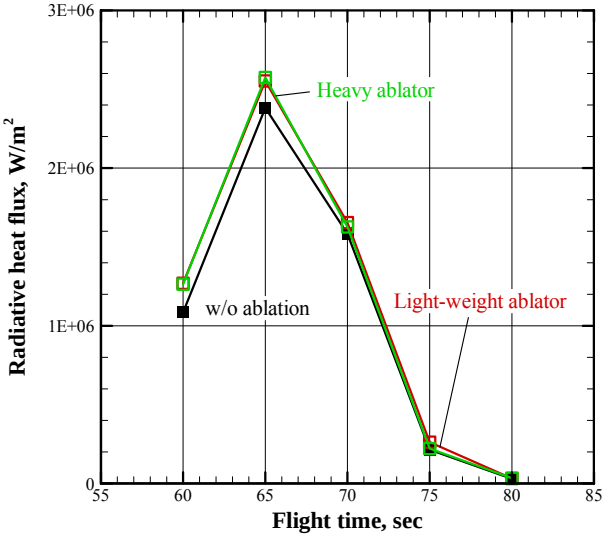

Figure 9. Time profiles of radiative heat flux at stagnation point.

Temperature distribution along center axis at each time is shown in **Figure 10**. The peak temperature is 3100 K for heavy ablator and 3200 K for light-weight ablator at 70 sec. The rear wall temperature does not rise until 80 sec. Though there is no heating, the rear wall temperature is increasing at 100 sec. On other hand, the rear wall temperature of heavy ablator keeps initial temperature. The light-weight ablator does not have enough thickness for this condition. However, it suggests that it can prevent heat by slightly increasing the thickness of the light-weight ablator. Present study calculated until 100 sec, because the heat flux became quite small estimated in ref. [26].

4. Concluding Remarks

A trajectory-based flow field simulation around Hayabusa capsule loaded light-weight ablator coupled with thermal response was carried out as a test case of near future mission. To validate this calculation, the conventional heavy ablator condition was carried out, too. The light-weight ablator in this calculation had been made and tested in our laboratory. In addition, the radiative heat flux had computed using 3-band model extended to nonequilibrium flow.

To calculate flow field around capsule, present simulation adopted four-temperature model and it was clear that the flow field had strong thermal nonequilibrium behind shock wave and thermo-chemical equilibrium near the

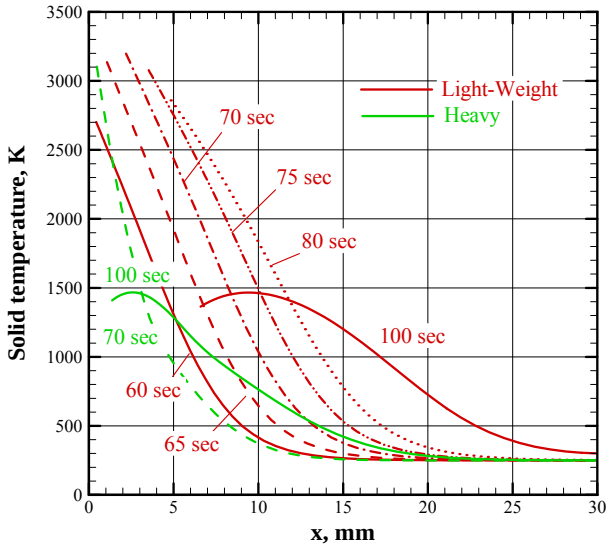

Figure 10. Temperature profiles along center axis.

wall surface. The precursor phenomenon could see using four-temperature model.

In thermal response for light-weight ablator, the state of the pyrolysis gas and its movement play important roles to the flow inside of ablator. The pyrolysis gas in heavy ablator flows towards a near boundary surface but the pyrolysis gas in light-weight ablator flows none one-dimensionally. The pyrolysis gas flow transports energies to the direction of rear wall and it makes the apparent heat conduction higher.

The difference of stagnation heat flux between heavy ablator and light-weight ablator is small. Especially radiated heat fluxes of these are almost the same. On the other hand, the stagnation heat flux taking account of the surface reaction becomes 30% larger than convectional heat flux without surface reaction.

The surface recession of light-weight ablator is few times larger than heavy ablator in addition; the heat transfer is slightly higher than heavy ablator. Therefore, this study shows light-weight ablator in this paper cannot use same configuration of heavy ablator and same thickness but it suggests that it can prevent heat by slightly increasing the thickness of the lightweight ablator.

5. Acknowledgements

The computation was mainly carried using the computer facilities at the Research Institute for Information Technology, Kyushu University. This work was partially supported by Grant-in-Aid for Scientific Research, No. 23460954, sponsored by Ministry of Education, Culture, Sports, Science and Technology, Japan.

REFERENCES

[1] T. Yamada, N. Ishii, Y. Inatani and M. Honda, "Thermal Protection System of the Reentry Capsule with Superorbital Velocity," Institute of Space and Astronautical Science Report Source Publishing No. 17, 2003, pp. 245-261.

[2] M. A. Covington, J. M. Heinemann, H. E. Goldstein, Y.-K. Chen, I. Terrazas-Salinas, J. A. Balboni, J. Olejniczak and E. R. Martinez, "Performance of a Low Density Ablative Heatshield Material," *Journal of Spacecraft and Rockets*, Vol. 45, No. 4, 2008, pp. 854-864.

[3] T. Yamada, Y. Ishida, T. Suzuki, K. Takasaki, K. Fujita, T. Ogasawara and T. Abe, "Development of High and Low Density Ablators for Dash-II and Future Reentry Missions," *Proceedings of the 27th International Symposium on Space Technology and Science*, Tsukuba, 5-12 July 2009, p. e-03.

[4] Y. K. Chen and F. S. Milos, "Ablation and Thermal Response Program for Spacecraft Heatshield Analysis," *Journal of Spacecraft and Rockets*, Vol. 36, No. 3, 1999, pp. 475-483.

[5] Y. K. Chen and F. S. Milos, "Two-Dimensional Implicit Thermal Response and Ablation Program for Charring Materials," *Journal of Spacecraft and Rockets*, Vol. 38, No. 4, 2001, pp. 473-481.

[6] H. Ahn, C. Park and K. Sawada, "Response of Heatshield Material at Stagnation Point of Pioneer-Venus Probes," *Journal of Thermophysics and Heat Transfer*, Vol. 16, No. 3, 2002, pp. 432-439.

[7] T. Suzuki, K. Sawada, T. Yamada and Y. Inatani, "Thermal Response of Ablative Test Piece in Arc-Heated Wind Tunnel," AIAA Paper No. 2004-0341, 2004.

[8] T. Suzuki, T. Sakai and T. Yamada, "Calculation of Thermal Response of Ablator under Arcjet Flow Condition," *Journal of Thermophysics and Heat Transfer*, Vol. 21, No. 2, 2007, pp. 257-266.

[9] S. Nozawa, T. Kanazaka, H. Kihara and K. Abe, "Experimental and Numerical Studies of Spallation Particles Ejected from A Light-Weight Ablator," *Proceedings of 61st International Astronautical Congress*, Prague, 27 September-1 October 2010, IAC-10-C2.7.7.

[10] Y. Takahashi, H. Kihara and K. Abe, "Effect of Radiative Heat Transfer in Arc-Heated Nonequilibrium Flow Simulation," *Journal of Physics D*: *Applied Physics*, Vol. 43, 2010, Article ID: 185201. doi:10.1088/0022-3727/43/18/185201

[11] N. Hirata, S. Nozawa, Y. Takahashi, H. Kihara and K. Abe, "Numerical Study of Pyrolysis Gas Flow and Heat Transfer inside an Ablator," *Computational Thermal Sciences*, Vol. 4, No. 3, 2012, pp. 225-242.

[12] C. Park, R. L. Jaffe and H. Partridge, "Chemical-Kinetic Parameters of Hyperbolic Earth Entry," *Journal of Thermophysics and Heat Transfer*, Vol. 15, No. 1, 2001, pp. 76-90.

[13] C. Park, "Rotational Relaxation of N_2 behind a Strong Shock Wave," *Journal of Thermophysics and Heat Transfer*, Vol. 18, No. 4, 2004, pp. 527-533. doi:10.2514/1.11442

[14] C. Park, "Problems of Rate Chemistry in the Flight Regimes of Aeroassisted Orbital Transfer Vehicles," AIAA Paper 84-1730, 1985.

[15] J. P. Appleton and K. N. C. Bray, "The Conservation Equations for a Nonequilibrium Plasma," *Journal of Fluid Mechanics*, Vol. 20, No. 4, 1964, pp. 659-672.

[16] P. A. Gnoffo, R. N. Gupta and J. L. Shinn, "Conservation Equations and Physical Models for Hypersonic Air Flows in Thermal and Chemical Nonequilibrium," National Aeronautics and Space Administration, Washington DC, 1989.

[17] S. S. Lazdinis and S. L. Petrie, "Free Electron and Vibrational Temperature Nonequilibrium in High Temperature Nitrogen," *Physics of Fluids*, Vol. 17, No. 8, 1974, pp. 1539-1546.

[18] J.-H. Lee, "Electron-Impact Vibrational Relaxation in High-Temperature Nitrogen," *Journal of Thermophysics and Heat Transfer*, Vol. 7, No. 3, 1993, pp. 399-405.

[19] T. Sakai, "Computational Simulation of High-Enthalpy Arc Heater Flows," *Journal of Thermophysics and Heat Transfer*, Vol. 21, No. 1, 2007, pp. 77-85.

[20] M. Yamada, Y. Matsuda, H. Hirata, Y. Takahashi, H.

Kihara and K. Abe, "Numerical Simulation of Flow Field and Heat Transfer around HAYABUSA Reentry Capsule," *Proceedings of the 28th International Symposium on Space Technology and Science*, Okinawa, 5-12 June 2011, p. e-38.

[21] Y. K. Chen and F. S. Milos, "Loosely Coupled Simulation for Two-Dimensional Ablation and Shape Change," *Journal of Spacecraft and Rockets*, Vol. 47, No. 5, 2010, pp. 775-785.

[22] T. Kanzaka, S. Nozawa, Y. Takahashi, H. Kihara and K. Abe, "Numerical Investigation of Thermal Response of Ablator Exposed to Thermochemical Nonequilibrium Flow," *Proceediongs of the 6th Asian-Pacific Conference on Aerospace Technology and Science*, Huangshan, 15-19 November 2009, B2-2.

[23] S. Gordon and B. J. McBridge, "Computer Program for Calculation of Complex Chemical Equilibrium Computation and Application," NASA Reference Publication 1311, 1994.

[24] R. L. Potts, "Application of Integral Methods to Ablation Charring Erosion: A Review," *Journal of Spacecraft and Rockets*, Vol. 32, No. 2, 1995, pp. 200-209.

[25] M. W. Chase Jr., C. A. Davies Jr., J. R. Downey, D. J. Frurip, R. A. McDonald and A. N. Syverud, "JANAF Thermochemical Tables," *Journal of Physical and Chemical Reference Data*, Vol. 14, 1985, pp. 535.

[26] T. Suzuki, K. Fujita, T. Yamada, Y. Inatani and N. Ishii, "Post-Flight TPS Analysis fo Hayabusa Reentry Capsul," AIAA Paper 2011-3759, 2011.

